Original scientific papers UDK 616.132.2-007.251
doi: 10.7251/COMEN1801001F

COMPUTER MODELING OF STENT DEPLOYMENT AND PLAQUE PROGRESSION IN THE CORONARY ARTERIES

Nenad Filipović[1,2], Velibor Isailović[1,2], Žarko Milosević[1,2], Dalibor Nikolić[1,2], Igor Saveljić[1,2], Tijana Đukić[1,2], Milica Nikolić[1,2], Bojana Cirković-Anđelković[1,2], Exarchos Themis[3], Dimitris Fotiadis[3], Gualtiero Pelosi[4], Oberdan Parodi[4]

[1] Faculty of Engineering, University of Kragujevac, Sestre Janjić 6, Kragujevac, Serbia
[2] BioIRC, Bioengineering Research and Development Center, Prvoslava Stojanovica 6, Kragujevac, Serbia
[3] Foundation of Research and Technology Hellas - Biomedical Research Institute, Ioannina, Greece, University of Ioannina, Ioannina, Greece
[4] Instituto di Fisiologia Clinica, Consiglio Nazionale delle Ricerche (IFC CNR), Pisa, Italy

Abstract: In this study stent deployment modeling with plaque formation and progression for specific patient in the coronary arteries are described. State of the art method for the reported investigations of blood flow in the stented arteries is described. In the method section, image segmentation method for arteries with stent is shortly described. Blood flow simulation is described with Navier-Stokes and continuity equation. Blood vessel tissue is modeled with nonlinear viscoelastic material properties. The coupling of fluid dynamics and solute dynamics at the endothelium was achieved by the Kedem-Katchalsky equations. The inflammatory process is modeled using three additional reaction-diffusion partial differential equations. Coupled method with mixed finite element and DPD (Dissipative Particle Dynamics) method is presented. In the results section, the examples with rigid and deformable arterial wall with stented and unstented arteries are presented. Effective stress analysis results for stent deployment have been shown. It can be seen that stent reduces wall shear stress significantly after deployment which is caused by opening the artery and reducing the narrowing. Some results for stent deployment model obtained with solver developed under PAK software package. These computer models can make better understanding and preparation of the surgeons for stent deployment in everyday clinical practice.

Keywords: stent deployment, numerical simulation, plaque progression, finite element method.

1. INTRODUCTION

CAD is the leading cause of death worldwide; it is on the rise and has become a true pandemic that respects no borders [1]. CAD has reached enormous proportions striking more and more at younger subjects. It is expected that in coming years, CAD linked with atherosclerosis will become the greatest epidemic to the mankind. Atherosclerosis involves the gradual development of fatty streaks in arterial walls into atheroma and characteristic plaques. The acute rupture of these atheromatous plaques causes local thrombosis, leading to partial or total occlusion of the affected artery. The clinical consequences of these plaques depend on their site and the degree and speed of vessel occlusion [2]. Among atherosclerosis, major clinical manifestations is the ischemic heart disease (IHD). IHD is a major cause of morbidity and mortality; only in UK, the annual deaths are 123,000 [3]. The associated direct and indirect costs of IHD are a major cost for the healthcare systems. Among the available treatment techniques are the percutaneous invasive interventions (PCIs), including percutaneous transluminal coronary angioplasty and stents implantation. In the

* Corresponding author: fica@kg.ac.rs

last decade there has been a steady and significant increase in the rate of stent implantation for IHD.

To reduce or remove obstructions inside arteries, like plaque formations, which block a normal blood flow and reduce oxygen supply to vital organs, angioplasty and stents were introduced to dilate the area of arterial blockage. The plaque is squeezed along the artery wall with the inflation of the balloon and the stent is implanted around the diameter of the artery. Stents can reduce the restenosis rate to 20–30% compared to balloon angioplasty [4]. Nowadays, coating stents with antiproliferative drugs seem to work well for patients since the restenosis rate decreases by 85% or more [5]. These drugs act by inhibiting neointimal proliferation. However, the drug can be delivered to the tissue only for a specific period of time, hence, the long term clinical outcome of such stents is still unknown.

While an implanted stent effectively enables a widening of the stenosed part of the blood vessel, it causes local injury to the vascular endothelium and also affects local haemodynamics in a manner conducive to growth of new tissue which is termed neointimal hyperplasia (NI) and subsequent restenosis [6], [7]. Recent evidence indicates that alterations in wall shear stress (WSS) distributions after stent implantation may represent an important contributing factor in the process of restenosis. Restenosis is the excessive growth of new tissue in the stented segment which can re-block the artery. The success of the stenting procedure depends on the severity of the restenosis. Neointimal hyperplasia was proved to be dependant on several factors including arterial injury, areas of flow induced low WSS less than 0.5 N/m2, areas of flow-induced high wall shear stress gradients (WSSG) higher than 200 N/m3, as well as other patient-specific medical factors such as diabetes mellitus [8], [9]. Non-uniform WSS within an arterial segment also affects the establishment of cell density gradients, gene expression, migration, and proliferation after vascular injury [10].

Many computational studies in the literature dealt with the influence of stent physical parameters on fluid dynamical changes correlated with the restenosis process [11-16]. Stent strut spacing, thickness and number of struts were found to influence the distribution of low and high shear stress values. However, the unrealistic assumption in the computational models that the stented artery is a simple cylindrical, rigid tube or even flat plane is implicit to most of these investigations. In reality, the coronary vasculature within which stents are commonly deployed exhibits a highly complex geometry with extensive curvature. This vessel curvature can have significant effect on the skewness of the velocity profile and the general behaviour of the flow in the stented segment.

A variety of studies was performed to compare steady-state vs. pulsatile flow simulations and investigated the effect of non-Newtonian blood properties on the resulting flow parameters. The pulsatile flow simulations showed in one investigation that the flow separation zones in the region between the stent wires also periodically increase and decrease in size. These results suggest that in pulsatile flow, the character of stent induced flow disturbance is highly dynamic. Some analyses revealed that while the non-Newtonian properties have a very limited impact on the global characteristics of the flow field, they do lead to a modest reduction in the size of the flow separation zone downstream of the stent [17−19].

In summary, there are strong limitations to the reported investigations of blood flow in stented arteries, mainly with respect to an idealised geometry of artery and stent. In this study, we firstly described section image segmentation method for arteries with stent. Then, numerical method for blood flow with mass transfer and plaque progression modeling is presented. Some of the results for stent deployment and plaque progression are described in the result section. Finally, a discussion and conclusion are given.

2. METHODS

2.1. Geometrical Stent Modelling

Voros et al. [20] presented a study for the evaluation of 3D quantitative measurements of coronary plaque by CTCA against IVUS. Another similar approach was introduced by Graaf et al. [21]. A semi-automated methodology for 3D reconstruction of arteries and their plaque morphology using CTCA was presented by Athanasiou et al. [22] showing that CTCA can be used for the accurate assessment and reconstruction of coronary arteries. Our method is able to reconstruct accurately a part of the arterial tree including lumen, outer wall calcified and non-calcified plaques.

3D Reconstruction and plaque characterisation tool will enable the 3D reconstruction of a vessel based on IVUS/OCT and angiography or CT. Fusion of angiography and IVUS mainly as well as OCT is a well-established technique. Bourantas et al. [23] developed an automated user-friendly system (ANGIOCARE), for rapid 3D coronary reconstruction, integrating angiographic and IVUS data. ANGIOCARE incorporates the method by Plissiti et al. [24-26] for border extraction. 3D Reconstruction

and plaque characterisation tool will extend this method also to incorporate the reconstruction of plaque lesions that are significant for accurate virtual stent deployment simulation.

3D Reconstruction and plaque characterisation tool will allow the semi-automatic stent reconstruction and evaluation of stent deployment. Deployment evaluation is well established for IVUS and OCT [27], [28] and will be included in the main functionalities of the 3D Reconstruction and plaque characterisation tool. The 3D Reconstruction and plaque characterisation tool provides the ability to detect automatically stent struts from OCT or IVUS modalities. Wang et al [29-31] presented a robust algorithm to process an entire IVOCT pullback run, which requires neither a priori status information, nor lumen or vessel wall contours. Accurate strut detection is the main requirement for extracting the stent deployment quantitative measurements. For stent deployment analysis with CTA imaging studies, the methodology presented for CTA reconstruction by Athanasiou et al [22] will be adapted. Our method extracts the interface of the stent (Figure 1) that will be used to extract the corresponding measures. Moreover, using the stent profile, ISR can also be evaluated.

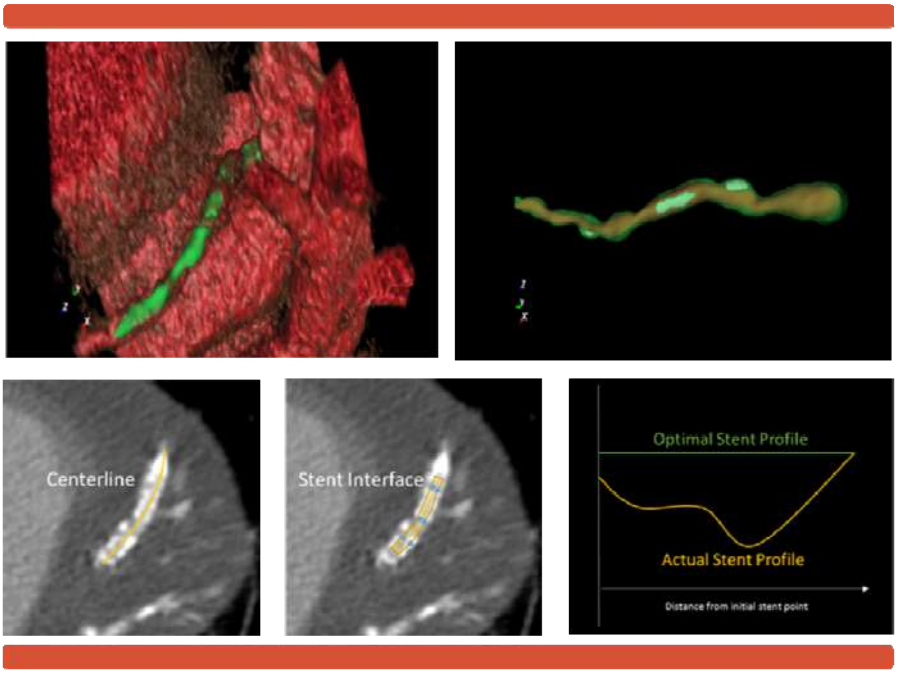

Figure 1. Volume rendering of heart with the vessel (green) superimposed and the 3D vessel with lumen (red), outer wall (green) and calcified plaques (white). Stent Profile Extraction. Initial stent centerline, stent interface extraction

3D Reconstruction and plaque characterisation tool will also be used in order to detect scaffold fracture (SF). According to Nakazawa [30], there are five (5) types of SF. Identification of types I and II are rather difficult [31] from any modality. Our method is focused on the semi-automatic detection of type III, IV and V SF fractures. The method will use the scaffold profiling method and strut detection in order to identify measures indicative of scaffold fracture. Those measures include the distance between neighboring struts, abrupt changes in scaffold centerline and other measures to estimate the probability of different SF types.

Currently, imaging studies (CCTA, IVUS, OCT and angiography) of the same patient, acquired at the same or two separate times, are interpreted separately. Our method will provide the tools to co-register imaging studies from the same or different modalities semi-automatically.

2.2. Blood flow simulation

In general, the sequence used to perform blood flow simulations is the acquisition of the 3D reconstructed model from the image modalities, the application of the appropriate input data and, finally, the acquisition of the desired output. Blood flow simulations are performed in three different categories of arteries: a) In unstented arteries assuming the walls to be rigid, b) in unstented arteries with deformable walls and c) in stented arteries with rigid walls.

The blood can be considered as an incompressible homogenous viscous fluid for flow in large blood vessels. Also, the laminar flow is dominant in

physiological flow environment. Therefore, the fundamental laws of physics which include balance of mass and balance of linear momentum are applicable here. These laws are expressed by continuity equation and the Navier-Stokes equations.

We here present the final form of these equations to emphasize some specifics related to blood flow. The incremental-iterative balance equation of a finite element for a time step 'n' and equilibrium iteration 'i' has a form

$$\begin{bmatrix} \frac{1}{\Delta t}\mathbf{M} + {}^{n+1}\tilde{\mathbf{K}}_{vv}^{(i-1)} & \mathbf{K}_{vp} \\ \mathbf{K}_{vp}^T & \mathbf{0} \end{bmatrix} \begin{Bmatrix} \Delta\mathbf{V}^{(i)} \\ \Delta\mathbf{P}^{(i)} \end{Bmatrix}_{blood} = \begin{Bmatrix} {}^{n+1}\mathbf{F}_{ext}^{(i-1)} \\ 0 \end{Bmatrix} - \begin{bmatrix} \frac{1}{\Delta t}\mathbf{M} + {}^{n+1}\mathbf{K}^{(i-1)} & \mathbf{K}_{vp} \\ \mathbf{K}_{vp}^T & 0 \end{bmatrix} \begin{Bmatrix} {}^{n+1}\mathbf{V}^{(i-1)} \\ {}^{n+1}\mathbf{P}^{(i-1)} \end{Bmatrix} + \begin{Bmatrix} \frac{1}{\Delta t}\mathbf{M}\,{}^{n}\mathbf{V} \\ 0 \end{Bmatrix} \quad (1)$$

where ${}^{n+1}\mathbf{V}^{(i-1)}$ ${}^{n+1}\mathbf{P}^{(i-1)}$ are the nodal vectors of blood velocity and pressure, with the increments in time step $\Delta\mathbf{V}^{(i)}$ and $\Delta\mathbf{P}^{(i)}$ (the index 'blood' is used to emphasize that we are considering blood as the fluid); Δt is the time step size and the left upper indices 'n' and 'n+1' denote start and end of time step; and the matrices and vectors are defined in [32]. Note that the vector ${}^{n+1}\mathbf{F}_{ext}^{(i-1)}$ of external forces includes the volumetric and surface forces. In the assembling of these equations, the system of equations of the form (1) is obtained, with the volumetric external forces and the surface forces acting only on the fluid domain boundary (the surface forces among the internal element boundaries cancel).

The specifics for the blood flow are that the matrix ${}^{n+1}\mathbf{K}^{(i-1)}$ may include variability of the viscosity if non-Newtonian behavior of blood is considered. We have that

$$\left[K_{KJ}^{(i-1)}\right]_{mk} = \left[\hat{K}_{KJ}^{(i-1)}\right]_{mk} + \int_V \mu^{(i-1)} N_{K,j} N_{J,j} dV \quad (2)$$

where $\mu^{(i-1)}$ corresponds to the constitutive law for the last known conditions (at iteration '$i-1$'). In case of use of the Cason relation (2), the second invariant of the strain rate $D_{II}^{(i-1)}$ is to be evaluated when computing $\mu^{(i-1)}$.

We note here that the penalty method can also be used, as well as the ALE formulation in case of large displacements of blood vessel walls [33].

In addition to the velocity and pressure fields of the blood, the distribution of stresses within the blood can be evaluated. The stresses ${}^{t}\sigma_{ij}$ at time 't' follow from

$${}^{t}\sigma_{ij} = -{}^{t}p\delta_{ij} + {}^{t}\sigma_{ij}^{\mu} \quad (3)$$

where

$${}^{t}\sigma_{ij}^{\mu} = {}^{t}\mu\left({}^{t}v_{i,j} + {}^{t}v_{j,i}\right) \quad (4)$$

is the viscous stress. Here, ${}^{t}\mu$ is viscosity corresponding to the velocity vector ${}^{t}\mathbf{v}$ at a spatial point within the blood domain. The field of the viscous stresses is given by (4).

Further, the wall shear stress at the blood vessel wall is calculated as:

$${}^{t}\tau = {}^{t}\mu\frac{\partial\,{}^{t}v_t}{\partial n} \quad (5)$$

where ${}^{t}v_t$ denotes the tangential velocity, and n is the normal direction at the vessel wall. Practically, we first calculate the tangential velocity at the integration points near the wall surface, and then numerically evaluate the velocity gradient $\partial\,{}^{t}v_t/\partial n$; finally, we determine the viscosity coefficient ${}^{t}\mu$ using the average velocity at these integration points. In essence, the wall shear stress is proportional to the shear rate γ at the wall, and the blood dynamic viscosity μ.

For a pulsatile flow, the mean wall shear stress within a time interval T can be calculated as [34]

$${}^{T}\tau_{mean} = \left|\frac{1}{T}\int_0^T {}^{t}\tau_n dt\right| \quad (6)$$

Another scalar quantity is a time-averaged magnitude of the surface traction vector, calculated as

$${}^{T}\tau_{mag} = \frac{1}{T}\int_0^T \left|{}^{t}\mathbf{t}\right| dt \quad (7)$$

where the vector ${}^{t}\mathbf{t}$ is given by the Cauchy formula.

2.3. Modeling the deformation of blood vessels

Blood vessel tissue has complex mechanical characteristics. The tissue can be modeled by using various material models, from linear elastic to nonlinear viscoelastic. We here summarize the governing finite element equations used in modeling wall tissue deformation with emphasis on implementation of nonlinear constitutive models.

The finite element equation of balance of linear momentum is derived from the fundamental differential equations of balance of forces acting at an elementary material volume. In dynamic analysis, we include the inertial forces in this equation accordingly. Then, by applying the principle of virtual work

$$\mathbf{M}\ddot{\mathbf{U}} + \mathbf{B}^{w}\dot{\mathbf{U}} + \mathbf{K}\mathbf{U} = \mathbf{F}^{ext} \quad (8)$$

Here the element matrices are: $\mathbf{M}$ is mass matrix; $\mathbf{B}^{w}$ is the damping matrix, in case when the material has a viscous resistance; $\mathbf{K}$ is the stiffness matrix; and $\mathbf{F}^{ext}$ is the external nodal force vector

which includes body and surface forces acting on the element. By the standard assembling procedure, the dynamic differential equations of motion are obtained. These differential equations can be further integrated in a way described, with a selected time step size Δt. The nodal displacements ${}^{n+1}\mathbf{U}$ at end of time step are finally obtained according to equation:

$$\hat{\mathbf{K}}_{tissue}\,{}^{n+1}\mathbf{U} = {}^{n+1}\hat{\mathbf{F}} \tag{9}$$

where the tissue stiffness matrix $\hat{\mathbf{K}}_{tissue}$ and vector ${}^{n+1}\hat{\mathbf{F}}$ are expressed in terms of the matrices and vector in (8). Note that this equation is obtained under the assumption that the problem is linear: displacements are small, the viscous resistance is constant, and the material is linear elastic.

In many circumstances of blood flow, the wall displacements can be large, as in case of aneurism or hart, hence the problem becomes geometrically nonlinear. Also, the tissues of blood vessels have nonlinear constitutive laws, leading to materially-nonlinear FE formulation. Therefore, the approximations adopted to obtain equation (9) may not be appropriate. For a nonlinear problem, instead of (9) we have the incremental-iterative equation

$${}^{n+1}\hat{\mathbf{K}}_{tissue}^{(i-1)}\,\Delta\mathbf{U}^{(i)} = {}^{n+1}\hat{\mathbf{F}}^{(i-1)} - {}^{n+1}\mathbf{F}^{\mathrm{int}(i-1)} \tag{10}$$

where $\Delta\mathbf{U}^{(i)}$ are the nodal displacement increments for the iteration 'i', and the system matrix ${}^{n+1}\hat{\mathbf{K}}_{tissue}^{(i-1)}$, the force vector ${}^{n+1}\hat{\mathbf{F}}^{(i-1)}$ and the vector of internal forces ${}^{n+1}\mathbf{F}^{\mathrm{int}(i-1)}$ correspond to the previous iteration.

We here emphasize the material nonlinearity of blood vessels which is used in further applications. As presented, the geometrically linear part of the stiffness matrix, $\left({}^{n+1}\mathbf{K}_L\right)_{tissue}^{(i-1)}$, and nodal force vector, ${}^{n+1}\mathbf{F}^{\mathrm{int}(i-1)}$, are defined in equation:

$$\left({}^{n+1}\mathbf{K}_L\right)_{tissue}^{(i-1)} = \int_V \mathbf{B}_L^T\,{}^{n+1}\mathbf{C}_{tissue}^{(i-1)}\mathbf{B}_L\,dV, \quad \left({}^{n+1}\mathbf{F}^{\mathrm{int}}\right)^{(i-1)} = \int_V \mathbf{B}_L^T\,{}^{n+1}\boldsymbol{\sigma}^{(i-1)}\,dV \tag{11}$$

where the consistent tangent constitutive matrix ${}^{n+1}\mathbf{C}_{tissue}^{(i-1)}$ of tissue and the stresses at the end of time step ${}^{n+1}\boldsymbol{\sigma}^{(i-1)}$ depend on the material model used. Calculation of the matrix ${}^{n+1}\mathbf{C}_{tissue}^{(i-1)}$ and the stresses ${}^{n+1}\boldsymbol{\sigma}^{(i-1)}$ for the tissue material models were used in further applications. In each of the subsequent sections we will give the basic data about the models used in the analysis.

2.4. Plaque formation and progression modelling – continuum approach

Continuum based methods is an efficient way for modelling the evolution of plaque. In our model, LDL concentration is first introduced into the system of partial differential equations as a boundary condition. The model simulates the inflammatory response formed at the initial stages of plaque formation.

Regarding the particle dynamics, the model is based on the involvement of LDL/oxidized LDL, monocytes and macrophages, and foam cells and extra cellular matrix. Reaction-diffusion differential equations are used to model these particle dynamics. The adhesion rate of the molecules depends on the local hemodynamics which is described by solving the Navier-Stokes equations. Intima LDL concentration is a function of the wall shear stress, while the adhesion of monocytes is a function of shear stress and VCAM. Finally, the alterations of the arterial wall are simulated. A finite element solver is used to solve the system of the equations. The lumen is defined as a 2D domain while the intima is simplified as 1D model due to its thin geometry. First, the LDL penetration to the arterial wall as well as the wall shear stress is calculated. Then the concentration of the various components of the model is calculated in order to simulate the intima fattening in the final step.

The LDL penetration is defined by the convection-diffusion equation, while the endothelial permeability is shear stress dependent. This model produces results about the initial stages of the atherosclerotic plaque formation. More specifically, concentration of LDL is calculated on the artery wall and in the next step also the oxidized LDL. Furthermore, monocytes and their modified form (macrophages) are also counted. Solution to the system provides to the user the concentration of foam cells created when a threshold on LDL concentration is reached.

The previous model describes the initial stages of atherosclerosis. However, atherosclerosis is characterized by the proliferation of SMCs. A medical user needs a prediction for the plaque formation which is based on the concentration of SMCs, the necrotic core and the extracellular matrix. In this respect, a new approach to count the concentration of SMCs is being developed. The user is also provided with results regarding the formation of plaque in an overall manner.

The fluid is assumed to be steady, incompressible and laminar for modeling fluid dynamics in the lumen. Navier-Stokes equations were used (12),(13)

$$-\mu\nabla^2 u_l + \rho\left(u_l\cdot\nabla\right)u_l + \nabla p_l = 0 \tag{12}$$

$$\nabla u_l = 0 \tag{13}$$

where u_l is blood velocity, p_l is pressure, μ is blood dynamic viscosity and ρ is blood density.

Darcy`s Law was used to model mass transfer across the wall (transmural flow) of the blood vessel.

$$u_w - \nabla\left(\frac{k}{\mu_p} p_w\right) = 0 \tag{14}$$

$$\nabla u_w = 0 \tag{15}$$

where u_w is transmural velocity, p_w pressure in the arterial wall, μ_p is viscosity of blood plasma, and k is the Darcian permeability coefficient of the arterial wall (14), (15). Convective diffusion equations were occupied for modeling mass transfer in the lumen (16)

$$\nabla\cdot\left(-D_l\nabla c_l + c_l u_l\right) = 0 \tag{16}$$

where c_l represents blood concentration in the lumen and D_l is diffusion coefficient of the lumen.

Convective diffusion reactive equations (17) were used for modeling mass transfer in the wall which are related to transmural flow.

$$\nabla\cdot\left(-D_w\nabla c_w + K c_w u_w\right) = r_w c_w \tag{17}$$

where c_w is solute concentration in the arterial wall, D_w is diffusive coefficient of solution in the wall, K is solute lag coefficient and r_w is consumption rate constant.

The coupling of fluid dynamics and solute dynamics at the endothelium was achieved by the Kedem-Katchalsky equations (18),(19).

$$J_v = L_p\left(\Delta p - \delta_d \Delta\pi\right) \tag{18}$$

$$J_s = P\Delta c + \left(1-\delta_f\right) J_v \bar{c} \tag{19}$$

where L_p is the hydraulic conductivity of the endothelium, Δc is the solute concentration difference across the endothelium, Δp is the pressure drop across the endothelium, Δπ is the oncotic pressure difference across the endothelium, σ_d is the osmotic reflection coefficient, σ_f is the solvent reflection coefficient, P is the solute endothelial permeability, and $\bar{c}$ is the mean endothelial concentration [35].

The inflammatory process is modeled using three additional reaction-diffusion partial differential equations [36]:

$$\begin{aligned}
&\partial_t O = d_1\Delta O - k_1 O\cdot M \\
&\partial_t M + div(v_w M) = d_2\Delta M - k_1 O\cdot M + S/(1+S) \\
&\partial_t S = d_3\Delta S - \lambda S + k_1 O\cdot M + \gamma(O - O^{thr})
\end{aligned} \tag{20}$$

where O is the oxidized LDL in the wall, M and S are concentrations in the intima of macrophages and cytokines, respectively; d_1, d_2, d_3 are the corresponding diffusion coefficients; λ and γ are degradation and LDL oxidized detection coefficients; and v_w is the inflammatory velocity of plaque growth [36,37].

2.5. Discrete approach

Blood flow in the small coupled domain within finite element mesh is viewed as a motion of the collection of DPD particles. Motion of each DPD particle is described by the following Newton law equation:

$$m_i \dot{\mathbf{v}}_i = \sum_j (\mathbf{F}_{ij}^C + \mathbf{F}_{ij}^D + \mathbf{F}_{ij}^R) + \mathbf{F}_i^{ext} \tag{21}$$

where m_i is the mass of particle "i"; $\dot{\mathbf{v}}_i$ is the particle acceleration as the time derivative of velocity; $\mathbf{F}_{ij}^C$, $\mathbf{F}_{ij}^D$, and $\mathbf{F}_{ij}^R$ are the conservative (repulsive), dissipative and random (Brownian) interaction forces, that particle "j" exerts on particle "i", respectively, provided particle "j" is within the radius of influence r_c of particle "i"; and $\mathbf{F}_i^{ext}$ is the external force exerted on particle "i", which usually represents gradient of pressure or gravity force as a driving force for the fluid domain [38]. Hence, the total interaction force $\mathbf{F}_{ij}$ (Figure 2) between the two particles is:

$$\mathbf{F}_{ij} = \mathbf{F}_{ij}^C + \mathbf{F}_{ij}^D + \mathbf{F}_{ij}^R \tag{22}$$

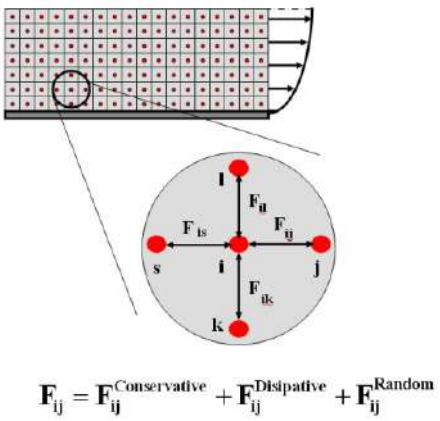

Figure 2. Interaction forces in the DPD approach

2.6. DPD modeling of oxidized LDL particle adhesion to the wall

When an oxidized LDL comes close to the wall and if shear rate allows, it binds to the wall. However, when adhered LDL particles are exposed simultaneously to other forces stronger than the binding forces, the bonds break. To incorporate LDL adhesion to vessel walls, we introduce an attractive (bonding) force, ($\mathbf{F}_{ij}^a$), in addition to the conservative, viscous and random interaction forces. As an approximation, we model the attractive force with a linear spring attached to the LDL's surface. The spring is attached to the vessel wall or to an already

adhered LDL particle. The effective spring constant for LDL adhesion on the vessel wall, or to another stationary LDL particle, is denoted by k_{bw}

The additional parameter involved in the model is the size of the domain from the LDL coated wall ($L_{\max}^{wall}$) for which the action of attractive force needs to be considered. We take the attractive force as

$$F_w^a = k_{bw}\left(1 - L_w / L_{\max}^{wall}\right) \tag{23}$$

where L_w is the distance of the oxidized LDL from the wall.

3. RESULTS

3.1. Coupled method for modelling of atherosclerosis

Coupled method for modelling of atherosclerosis assumed combination of continuum (finite element method) and discrete (DPD method) described in the previous section. Atherosclerosis development for specific patient at right coronary artery was simulated. Upstream of the bifurcation level, there was plaque progression. (Figure 3). The results give better insight in the microlevel approach for plaque progression.

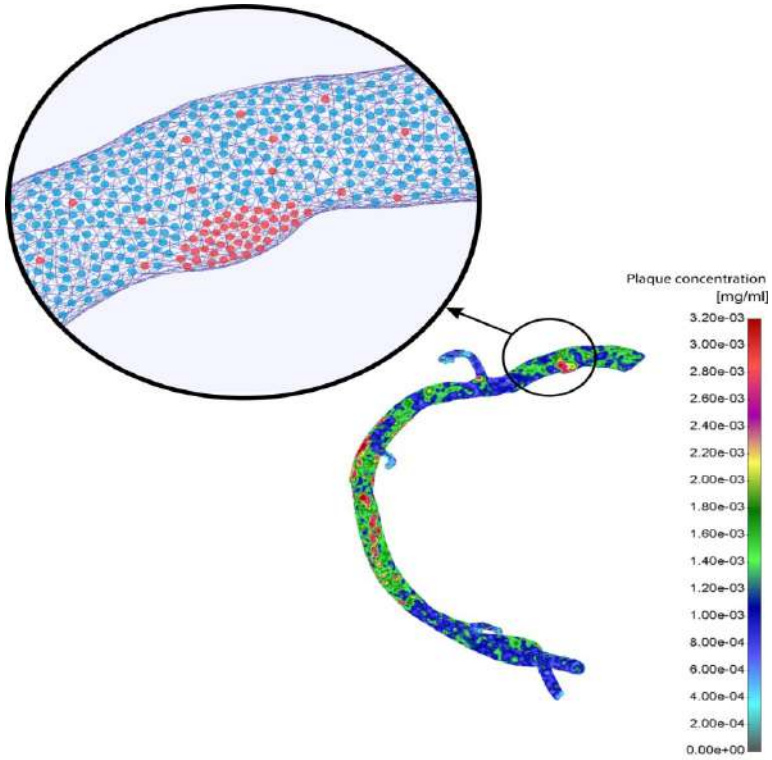

Figure 3. The right coronary artery for specific patient. Coupled simulation finite element and DPD method

3.2. Stent deployment modeling

The system of stent deployment which consists of three parts is modelled: balloon, stent and blood vessel. The first part – elastic balloon should be inflated in order to open stent and blood vessel with stenosis. The second part is stent, wired structure that should open and hold the blood vessel narrowed. Third part is blood vessel with narrowing caused by plaque progression.

Model contains of 8-node brick linear finite elements. Materials of all three structures are linearly elastic but with large deformations. Boundary conditions applied in this model are fixed nodes at the beginning and at the end of the blood vessel with stenosis, prescribed pressure in the balloon and symmetry boundary conditions at all three parts of the finite element mesh (because we modeled half of model based on symmetry assumption). Value of the pressure is not significant in this case, because it is fitted only to open stenosis. The pressure increases during the time linearly. Simulation has 200-time steps of 5 milliseconds. Besides the mentioned number of 3D finite elements, when the balloon and stent are in contact, or when stent and blood vessel is in contact, there is a variable number of elastic support elements, which depends on the contact area size between 3D elements in contact.

The initial results for stent deployment model obtained with solver developed under PAK software package are presented [51]. PAK software is upgraded with contact algorithm developed during this

study. The initial model is parametric, as explained in the previous section.

The results for stent opened by inflated balloon are given in Figure 4. There are two time steps: time step 10 and 160. Those two steps are characteristic because in time step 10, there appears contact between elastic balloon and stent, and in time step 160 the narrowed blood vessel is completely opened by balloon and stent. As it can be seen from images, at the beginning of simulation there is no contact between elastic balloon and stent, and only balloon has deformation. In time step 10, the contact appears, and balloon starts with opening of stent and also blood vessel. At the time step 160, diameter of blood vessel in narrowing is restored to original dimension.

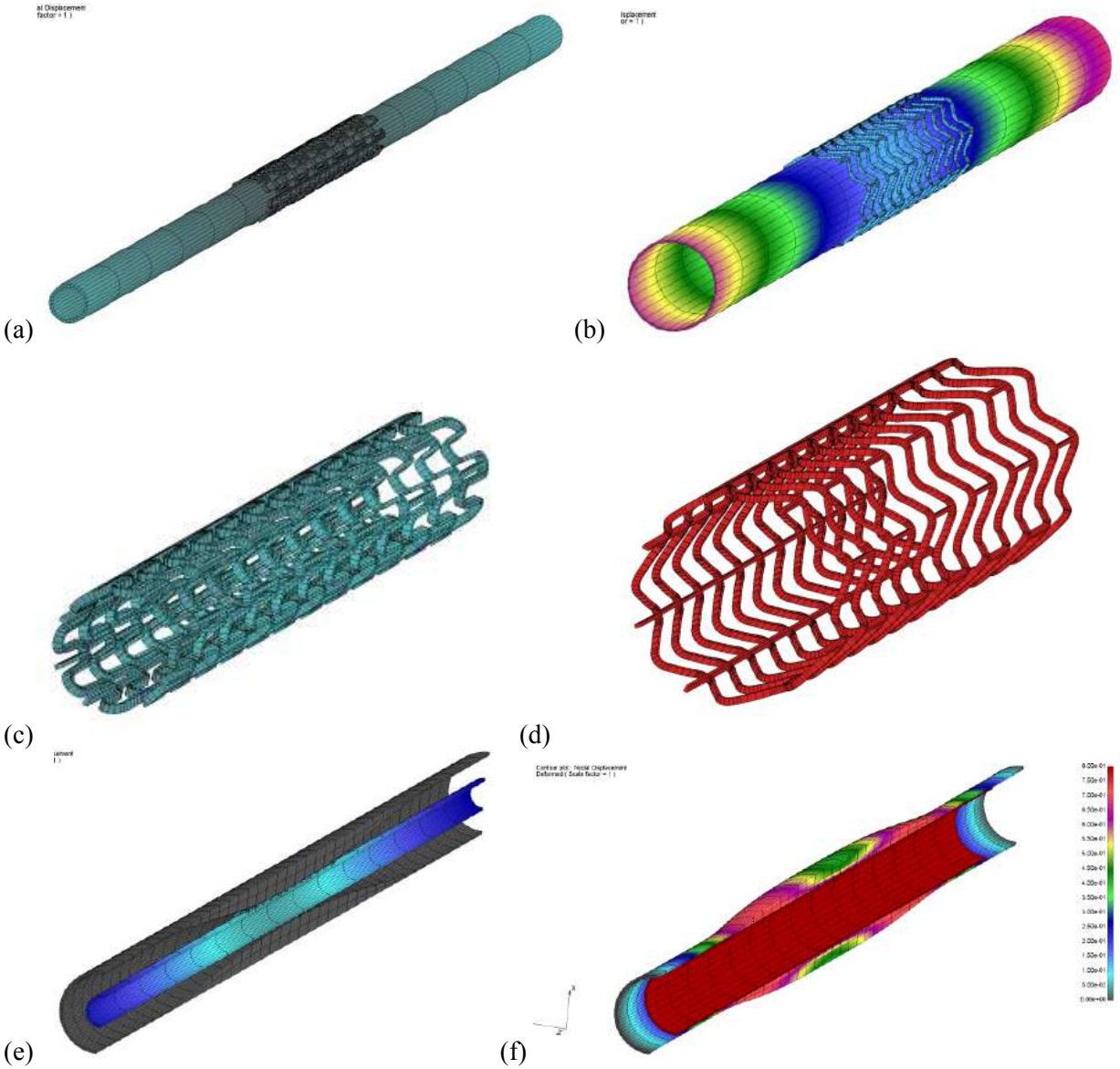

Figure 4. Results with parametric model: displacements field for: stent with balloon: (a) time step 10 and (b) time step 160; stent (c): time step 10 and (d) time step 160; whole model: (e) time step 10 and (f) time step 160

3.3. Stress analysis for stent deployment

According to the boundary conditions and loads mentioned above, the numerical analysis of the material behavior of this complex model is performed. To examine different loading conditions, we apply hemodynamic flow as well as stent deployment procedure at the arterial wall.

The stent is loaded by an internal uniform radial pressure linearly which varies from zero to 1 MPa. Due to the artery incompressibility requirement and to avoid locking-problems, 8-node brick elements are used in all the analyses [19]. In particular, in the simulations we use up to 232214 elements and 257532 nodes, resulting in 666354 variables. The interaction between the expanding stent and the artery is described as contact between

deformable surfaces. As contact conditions, we set finite sliding, no-friction, with the constraint enforced by a Lagrange multiplier method. The stenotic segment of the artery which was examined before and after stent deployment is presented in Figure 5.

The effective von Mises stress distribution in the stent is presented in Figure 6. It can be observed that highest stresses are located near the connectors between the stent struts. These parts are subjected to plastic deformation with maximal stress around 180 MPa.

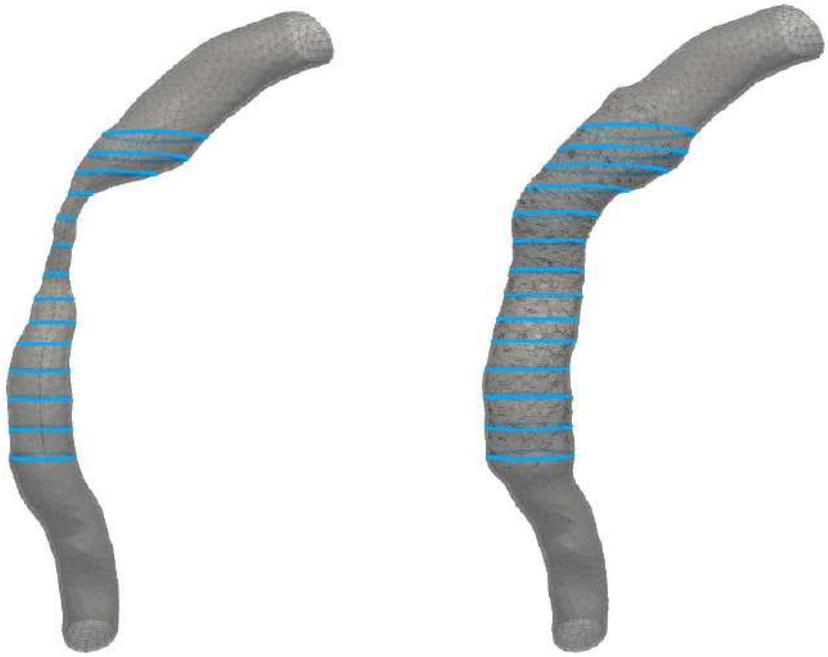

a) b)

Figure 5. Stent positioning before (a) and after (b) stent deployment

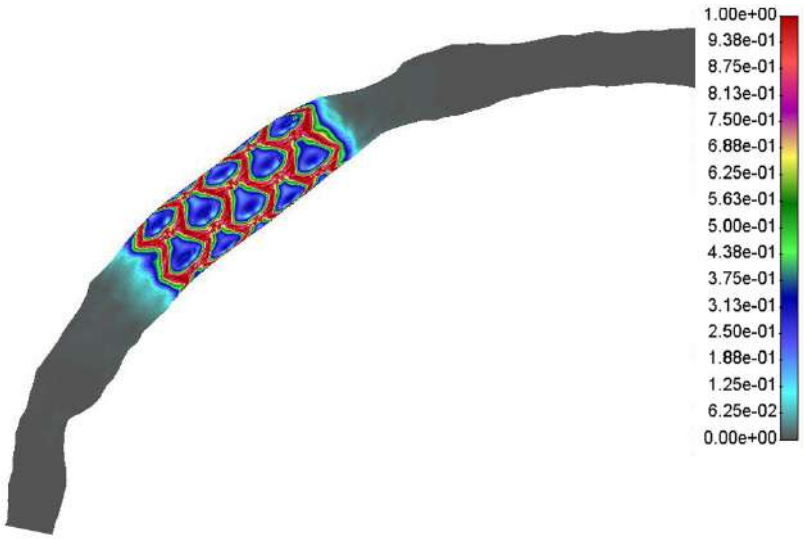

Figure 6. Effective stress distribution inside the arterial wall after stent deployment. The units are in MPa.

The effective stress distribution in the arterial wall at the two different cross-section locations at the end of stent deployment with maximum deployment pressure is shown in Figure 7. It can be observed that higher stress exists when wall thickness is reduced during deployment procedure.

Stent forces distribution in the arterial wall for the inflation pressure 1 kPa for stent deployment in the coronary artery is presented in Figure 8.

Von Mises stress distribution in the arterial wall for the inflation pressure 1 kPa for stent deployment in the coronary artery is presented in Figure 9.

These results for stent forces and Von Mises stress in the arterial wall during stent deployment can be very useful for prediction of the restenosis process.

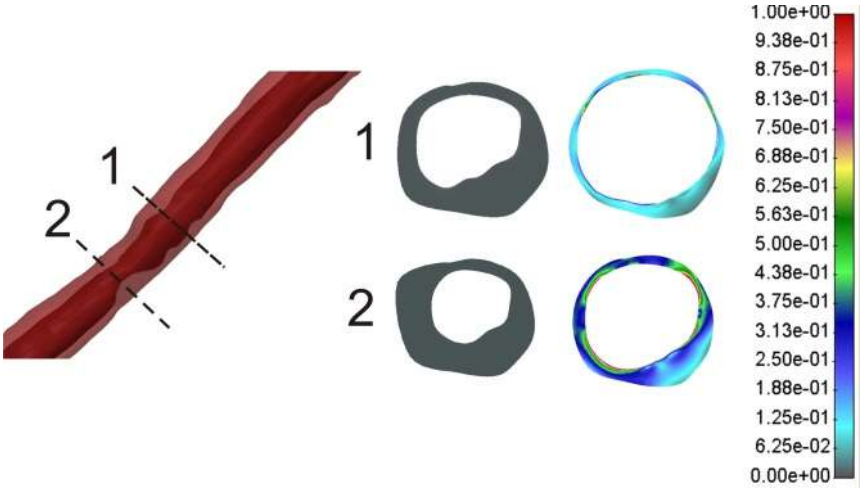

Figure 7. Effective stress distribution in the two different cross-section locations inside the arterial wall at the end of stent deployment

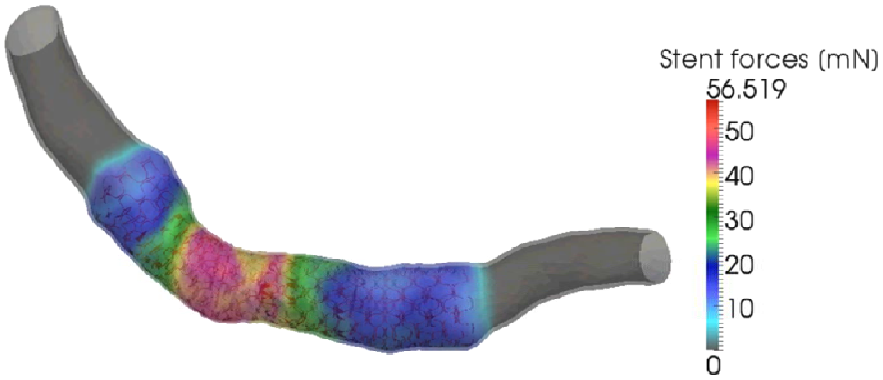

Figure 8. Stent deployment in the coronary artery. Stent forces distribution in the arterial wall for the inflation pressure 1 kPa

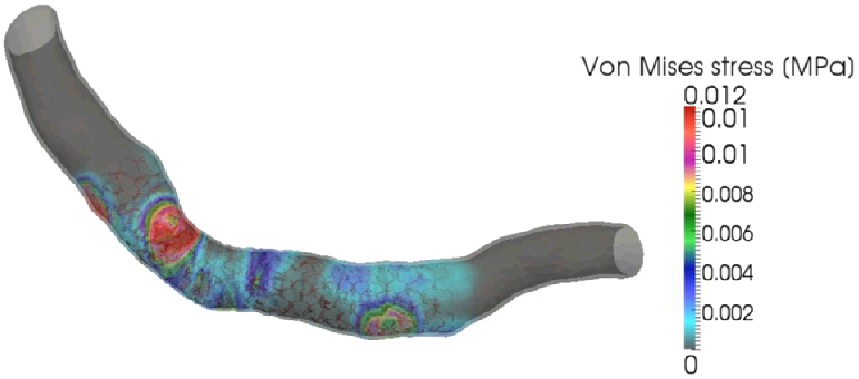

Figure 9. Stent deployment in the coronary artery. Von Mises stress distribution in the arterial wall for the inflation pressure 1 kPa

3.4. Plaque concentration for stented arteries

3D simulation of blood flow through lumen and plaque progression in vessel wall was simulated. The bio molecular parameters such as LDL, HDL and triglycerides are used for the computer simulation, as well as adhesion molecules ICAM1, VCAM1 and E-Selectin (Tab. 1).

Results of first numerical simulation (baseline) are presented in Figure 10.

Table 1. The bio molecular parameters and adhesion molecules

Time	LDL	HDL	Triglycerides	ICAM1	VCAM1	E-Selectin
Baseline	118	37	172	166.19	557.17	26
Follow-up 1	/	/	/	128.93	483.37	22.62
Follow-up 2	55	57	178	142.23	587.72	/

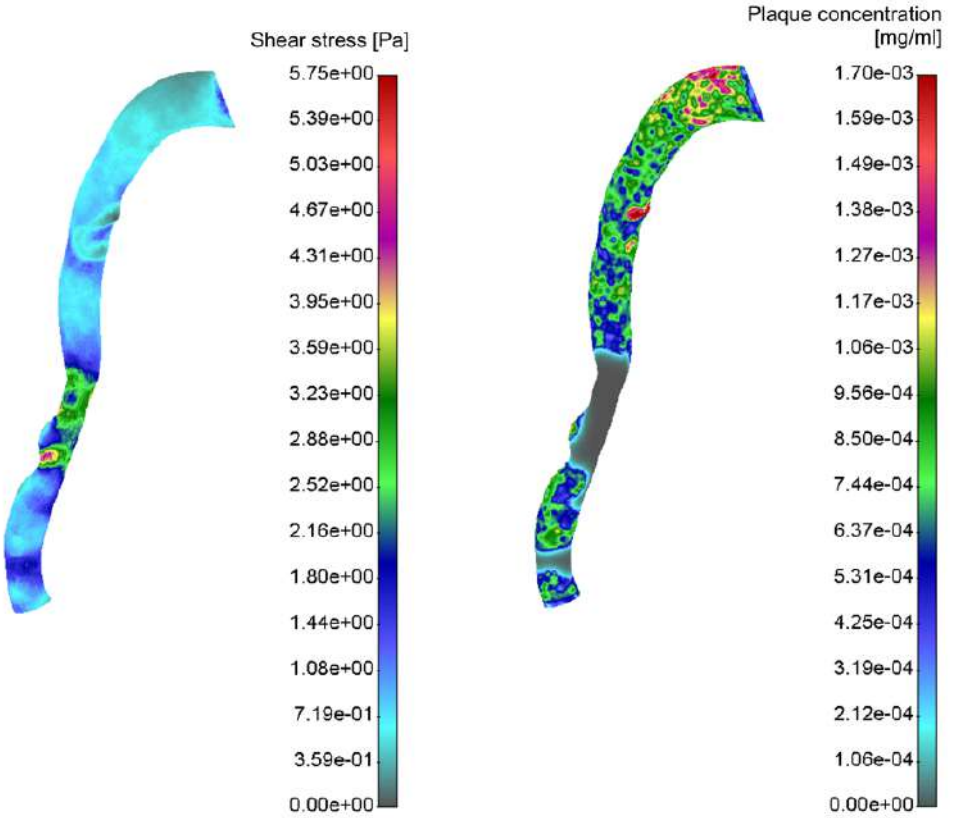

Figure 10. Shear stress distribution (left) and plaque concentration (right) for baseline

At a length of 1 to 4 mm, from the inlet of the coronary artery, a low value of wall shear stress was observed. Average values range from 0.23 to 0.36 Pa, measured at cross sections, at a distance of 0.5 mm. At 15.8 mm from the beginning of the artery, a low shear stress was also noticed. Low shear stress values are associated with increased plaque concentration, as shown in the Figure 10 (right). The highest values of plaque concentration in these zones are 1.7e-03 mg/ml.

The result of numerical simulation for the second time – follow-up 1 are presented in the Figure 11.

Further development of plaque concentrations was observed in the areas where low shear stress appears, there is an increase in these values, and the range of these values is from 0.31 to 0.39 Pa. It can be seen that the area of plaque concentration is expanding (Fig 11, right).

The third numerical simulation presents the condition of the artery after 6 years (Figure 12). Average values of shear stress in the observed zones of the artery range from 0.43 to 0.47 Pa. Also, it is clear from Figure 12 (right) that there has been a significant increase in the plaque development in the observed zones.

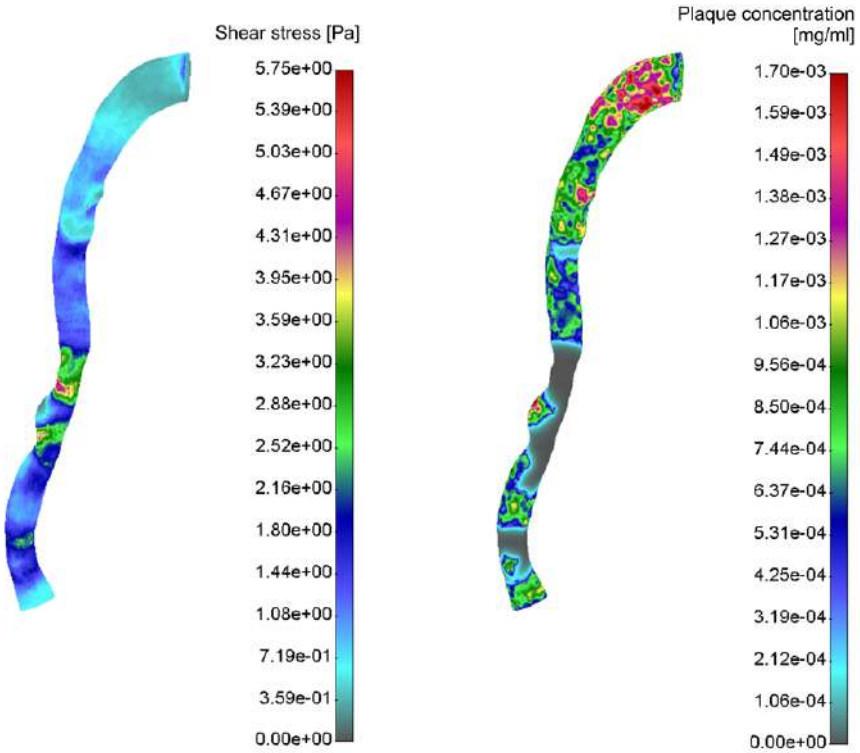

Figure 11. Shear stress distribution (left) and plaque concentration (right) for follow-up 1

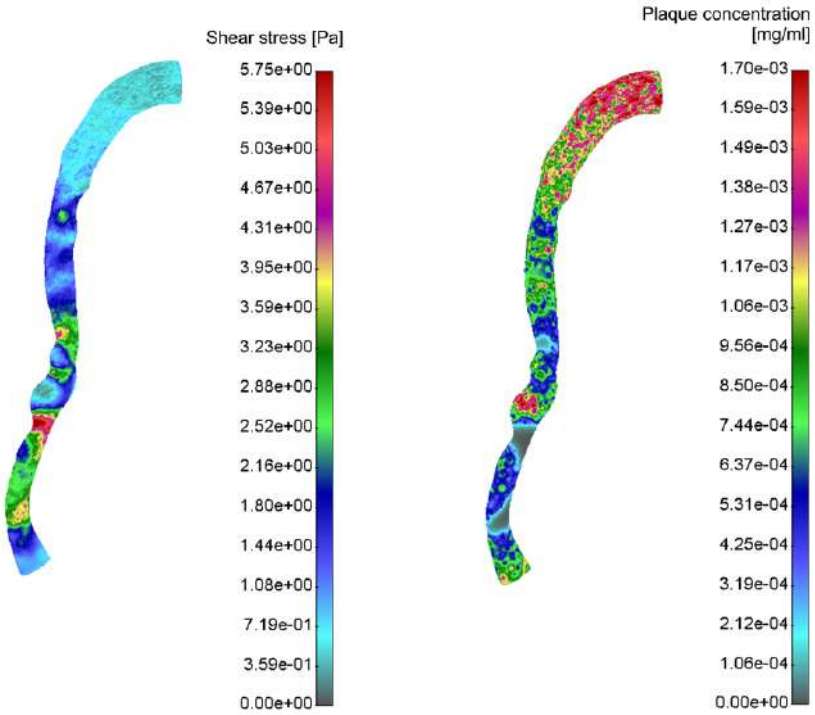

Figure 12. Shear stress distribution (left) and plaque concentration (right) for follow-up 2

4. DISCUSSION AND CONCLUSIONS

In this study, plaque formation and progression model for coronary artery with stent deployment modelling for specific patient is analyzed. A coupled 3D artery reconstruction from IVUS and Angiography image modalities, with ability of detection of luminal narrowing, on one side, and generating finite element models and processing them, on the other side, is described. The geometry of the patients for baseline and follow-up has been used with detailed described image techniques. The flow equations are coupled with the transport equation applying realistic boundary conditions for each patient.

Blood flow simulation is described with Navier-Stokes and continuity equation. The governing finite element equations used in modeling wall tissue deformation with emphasis on implementation of nonlinear constitutive models are described. The coupling of fluid dynamics and solute dynamics at the endothelium was achieved by the Kedem-Katchalsky equations.

Discrete approach used DPD method with conservative, dissipative and random forces and additional attractive force to the arterial wall. Some of initial results are presented for a few patients for the left and right coronary artery. Biomolecular parameters ICAM1, LDL, HDL and Triglycerides for both patients are used to calculate plaque concentration. The follow up study of CT after 24 months was compared to simulation results. A good agreement was achieved. This methodology could be validated with retrospective studies from literature if at least two points in time are available (baseline and follow up).

Stress distribution of the artery wall and stent during expansion of occluded zones is analyzed. Also stent forces and Von Mises stress distribution after stent deployment is presented. Better understanding of stent deployment procedure and arterial wall response as well as arterial wall restenosis can be obtained using computer simulation.

5. ACKNOWLEDGMENT

This study was funded by the grants from the Serbia III41007, ON174028 and EC HORIZON2020 689068 SMARTool project.

6. REFERENCES

[1] The global burden of coronary heart disease | Medicographia (2015).

[2] W. Herrington, B. Lacey, P. Sherliker, J. Armitage, and S. Lewington, *Epidemiology of Atherosclerosis and the Potential to Reduce the Global Burden of Atherothrombotic Disease*, Circulation Research, Vol. 118−4 (2016) 535–546.

[3] C. Meads, C. Cummins, K. Jolly, A. Stevens, A. Burls, and A. Hyde, *Coronary artery stents in the treatment of ischaemic heart disease: a rapid and systematic review*, Health Technol Assess, Vol. 4−23 (2000) 1–153.

[4] D. L. Fischman, M. B. Leon, D. S. Baim, R. A. Schatz, M. P. Savage, I. Penn, K. Detre, L. Veltri, D. Ricci, M. Nobuyoshi, M. Cleman, R. Heuser, D. Almond, P. S. Teirstein, R. D. Fish, A. Colo, *A randomized comparison of coronary-stent placement and balloon angioplasty in the treatment of coronary artery disease.* N. Engl. J. Med., Vol. 331 (1994) 496−501.

[5] M. C. Morice, P. W. Serruys, J. E. Sousa, J. Fajadet, B. Hayashi, M. Perin, A. Colombo, G. Schuler, P. Barragan, G. Guagliumi, F. Molnàr *A Randomized Comparison of a Sirolimus-Eluting Stent With a Standard Stent For Coronary Revascularization.* N.Engl. Med Vol. 349 (2002) 1315−1323.

[6] V. S. Newman, J. L. Berry, W. D. Routh, C.M. Ferrario, R.H. Dean, *Effects of vascular stent surface area and hemodynamics on intimal thickening*. J. vasc. Interv. Radiol., Vol. 7 (1996) 387−393.

[7] T. Murata, T. Hiro, T. Fujii, K. Yasumoto, A. Murashige, M. Kohno, J. Yamada, T. Miura, M. Matsuzaki, *Impact of the cross-sectional geometry of the post-deployment coronary stent on in-stent neoinimal hyperplasia: an intravascular ultrasound study*. Circ. J., Vol. 66 (2002) 489−493.

[8] J. Murphy, F. Boyle, *Assessment of the effects of increasing levels of physiological realism in the computational fluid dynamics analyses of implanted coronary stents*. 3th Annual International IEEE EMBS Conference (2008).

[9] N. DePaola, M. A. J. Gimbrone, P. F. Davies, C. F. Dewey, *Vascular endothelium responds to fluid shear stress gradients*. Arterioscler. Thromb., Vol. 12 (1992) 1254−1257.

[10] R. Balossino, F. Gervaso, F. Migliavacca, G. Dubini, *Effects of different stent designs on local hemodynamics in stented arteries*. Journal of Biomechanics, Vol. 41 (2008) 1053−1061.

[11] Y. He, N. Duraiswamy, A. O. Frank, J. E. Moore Jr., *Blood Flow in Stented Arteries: A Parametric Comparison in Three-Dimensions*. Journal of Biomechanical Engineering. Vol. 22 (2005) 637–647.

[12] S. Natarajan, M. R. Mokhtarzadeh-Dehghan, *A numerical and experimental study of periodic flow in a model of a corrugated vessel with application to stented arteries*, Medical Engineering & Physics, Vol. 22 (2000) 555–566.

[13] J. F. LaDisa, I. Guler, L. E. Olson, D. A. Hettrick, J. R. Kersten, D. C. Warltier, P. S. Pagel, *Three-Dimensional Computational Fluid Dynamics Modeling of Alterations in Coronary Wall Shear Stress Produced by Stent Implantation*, Annals of Biomedical Engineer, Vol. 31 (2003) 972−980.

[14] T. Seo, L. G. Schachter, A. I. Barakat, *Computational Study of Fluid Mechanical Disturbance Induced by Endovascular Stents*, Annals of Biomedical Engineering, Vol. 33−4 (2005) 444–456.

[15] A. Tortoriello, G. Pedrizzetti, *Flow-tissue interaction with compliance mismatch in a model*

stented artery. Journal of Biomechanics. Vol. 37 (2004) 1–11.

[16] J. L. Berry, A. Santamarina, K. E. Moore, S. Roychowdhury, W. D. Routh, *Experimental and Computational Flow Evaluation of Coronary Stents*. Annals of Biomedical Engineering Vol. 28 (2000) 386–398.

[17] J. F. LaDisa, L. E. Olson, H. E. Douglas, D. C. Warltier, J. R. Kersten, P. S. Pagel, *Alterations in regional vascular geometry produced by theoretical stent implantation influence distributions of wall shear stress: analysis of curved artery using 3D computational fluid dynamics models*. Biomed Eng Online, Vol. 16−5 (2006) 40.

[18] J. F. LaDisa, L. E. Olson, I. Guler, D. A. Hettrick, J. R. Kersten, D. C. Warltier, P. S. Pagel, *Circumferential vascular deformation after stent implantation alters wall shear stress evaluated with time-dependent 3D computational fluid dynamics models*. J. Appl Physiol., Vol. 98 (2005) 947−957.

[19] D. Rajamohan, R. K. Banerjee, L. H. Back, A. A. Ibrahim, M. A. Jog, *Developing Pulsatile Flow in a Deployed Coronary Stent*. Journal of Biomechanical Engineering, Vol. 128 (2006) 347−359.

[20] S. Voros et al. *Prospective validation of standardized, 3-dimensional, quantitative coronary computed tomographic plaque measurements using radiofrequency backscatter intravascular ultrasound as reference standard in intermediate coronary arterial lesions: results from the ATLANTA (assessment of tissue characteristics, lesion morphology, and hemodynamics by angiography with fractional flow reserve, intravascular ultrasound and virtual histology, and noninvasive computed tomography in atherosclerotic plaques) I study*, JACC Cardiovasc Interv, Vol. 4−2 (2011) 198–208.

[21] M. A. de Graaf et al., *Automatic quantification and characterization of coronary atherosclerosis with computed tomography coronary angiography: cross-correlation with intravascular ultrasound virtual histology*, Int J Cardiovasc Imaging, Vol. 29−5 (2013) 1177–1190.

[22] L. Athanasiou et al. *Three-dimensional reconstruction of coronary arteries and plaque morphology using CT angiography – comparison and registration with IVUS*, BMC Med Imaging, (2016) 16.

[23] C. V. Bourantas et al. *ANGIOCARE: an automated system for fast three-dimensional coronary reconstruction by integrating angiographic and intracoronary ultrasound data*, Catheter Cardiovasc Interv, Vol. 72−2 (2008) 166–175.

[24] M. E. Plissiti, D. I. Fotiadis, L. K. Michalis, and G. E. Bozios, *An Automated Method for Lumen and Media-adventitia Border Detection in a Sequence of IVUS Frames*, Trans. Info. Tech. Biomed., Vol. 8-2 (2004) 131–141.

[25] P. de Jaegere et al. *Intravascular ultrasound-guided optimized stent deployment. Immediate and 6 months clinical and angiographic results from the Multicenter Ultrasound Stenting in Coronaries Study (MUSIC Study)*, Eur. Heart J., Vol. 19−8 (1998) 1214–1223.

[26] P. C. Magnus et al. *Optical coherence tomography versus intravascular ultrasound in the evaluation of observer variability and reliability in the assessment of stent deployment: the OCTIVUS study,* Catheter Cardiovasc Interv, Vol. 86−2 (2015) 229–235.

[27] Y. Zhang et al. *Comparison of intravascular ultrasound versus angiography-guided drug-eluting stent implantation: a meta-analysis of one randomised trial and ten observational studies involving 19,619 patients*, EuroIntervention, Vol. 8−7 (2012) 855–865.

[28] S. Brugaletta et al. *Comparison of in vivo eccentricity and symmetry indices between metallic stents and bioresorbable vascular scaffolds: insights from the ABSORB and SPIRIT trials*, Catheter Cardiovasc Interv, Vol. 79−2 (2012) 219–228.

[29] A. Wang et al. *Automatic stent strut detection in intravascular optical coherence tomographic pullback runs*, Int J Cardiovasc Imaging, Vol. 29−1 (2013) 29–38.

[30] G. Nakazawa et al. *Incidence and predictors of drug-eluting stent fracture in human coronary artery a pathologic analysis*, J. Am. Coll. Cardiol., Vol. 54−21 (2009) 1924–1931.

[31] D. Scheinert et al. *Prevalence and clinical impact of stent fractures after femoropopliteal stenting*, J. Am. Coll. Cardiol., Vol. 45−2 (2005) 312–315.

[32] M. Kojic, N. Filipovic, B. Stojanovic, N. Kojic, *Computer Modeling in Bioengineering: Theoretical Background, Examples and Software*, John Wiley and Sons, Chichester, England (2008).

[33] N. Filipovic, S. Mijailovic, A. Tsuda, M. Kojic, *An Implicit Algorithm Within The Arbitrary Lagrangian-Eulerian Formulation for Solving Incompressible Fluid Flow With Large Boundary Motions*. Comp. Meth. Appl. Mech. Engrg. Vol. 195 (2006) 6347−6361.

[34] C.A. Taylor, T.J.R. Hughes, C.K. Zarins *Finite element modeling of blood flow in arteries*, Comp. Meth. Appl. Mech. Engrg., Vol. 158 (1998) 155−196.

[35] S. Nanfeng, W. Nigel, H. Alun, T. X. Simon, X. Yun, *Fluid-Wall Modelling of Mass Transfer in an Axisymmetric Stenosis: Effects of*

Shear-Dependent, Transport Properties Vol. 34 (2006) 1119–1128.

[36] N. Filipovic, M. Rosic, I. Tanaskovic, Z. Milosevic. D. Nikolic, N. Zdravkovic, A. Peulic, D. Fotiadis, O. Parodi, *ARTreat project: Three-dimensional Numerical Simulation of Plaque Formation and Development in the Arteries*, IEEE Trans Inf Technol Biomed. PMID: 21937352, (2011).

[37] N. Filipovic PAK-Athero, Finite Element Program for plaque formation and development. University of Kragujevac, Serbia, (2013).

[38] K. Boryczko, W. Dzwinel and D. Yuen *Dynamical clustering of red blood cells in capillary vessels,* J Mol Model, Vol. 9 (2003) 16−33.

КОМПЈУТЕРСКИ МОДЕЛ УГРАДЊЕ СТЕНТОВА И РАСТ ПЛАКА
У КОРОНАРНИМ АРТЕРИЈАМА

Сажетак: У раду је приказано моделирање уградње стента и симулација формирања и прогресије плака код појединачних пацијената са коронарним артеријама. Прво су описане најновије методе за симулацију струјања крви кроз артерије са стентовима. У секцији методе обрада слика артерија са стентовима је прво описана. Струјање крви је описано Навије−Стоксовом једначином и једначином континуитета. Зидови крвних судова су моделирани са нелинеарним високоеластичним материјалним моделом. Спрезање динамике флуида и транспортних једначина на зиду ендотелијуму описано је Кедем−Качалски једначинама. Инфламаторни процес моделиран је додатним реакционо-дифузним једначинама. Спрегнути метод који комбинује метод коначних елемената и ДПД је приказан. У секцији резултати приказани су неки примери крутих и деформабилних артеријских зидова са и без стента. Презентован је ефективни напон у самом стенту приликом његове уградње у коронарну артерију. Модели су рађени са домаћим софтверским пакетом ПАК. Ови компјутерски модели могу допринети бољем разумевању и припреми хирурга приликом уградње стентова у свакодневној клиничкој пракси.

Кључне ријечи: уградња стентова, нумеричка симулација, раст плака, метод коначних елемената.